Available online at www.sciencedirect.com
ScienceDirect
Trans. Nonferrous Met. Soc. China 28(2018) 1887−1902
Transactions of Nonferrous Metals Society of China
www.tnmsc.cn

Thermal kinetic analysis of a complex process from a solid-state reaction by deconvolution procedure from a new calculation method and related thermodynamic functions of $Mn_{0.90}Co_{0.05}Mg_{0.05}HPO_4{\cdot}3H_2O$

Chuchai SRONSRI, Banjong BOONCHOM

Advanced Phosphate Materials and Alternative Fuel Energy Research Unit, Department of Chemistry, Faculty of Science, King Mongkut's Institute of Technology Ladkrabang, Bangkok, Thailand

Received 18 October 2017; accepted 8 March 2018

Abstract: Three individual peaks of thermal solid-state reaction processes of the synthesized $Mn_{0.90}Co_{0.05}Mg_{0.05}HPO_4{\cdot}3H_2O$ were observed corresponding to dehydration I, dehydration II and polycondensation processes. An alternative method for the calculation of the extent of conversion was proposed from the peak area of the individual DTG peak after applying the best fitting deconvolution function (Frazer–Suzuki function). An iterative integral isoconversional equation was used to compute the values of the apparent activation energy E_α and they were found to be 65.87, 78.16 and 119.32 kJ/mol for three peaks, respectively. Each individual peak was guaranteed to be a single-step kinetic system with its unique kinetic parameters. The reaction mechanism functions were selected by the comparison between experimental and model plots. The results show that the first, second and final individual peaks were two-dimensional diffusion of spherical symmetry (D_2), three-dimensional diffusion of spherical symmetry (D_3) and contracting cylinder (cylindrical symmetry, R_2) mechanisms. Pre-exponential factor values of 3.91×10^6, 1.35×10^7 and 2.15×10^7 s^{-1} were calculated from the E_α values and reaction mechanisms. The corresponded standard thermodynamic functions of the transition-state (activated) complexes were determined and found to agree well with the experimental data.

Key words: solid-state reaction; calculation method; complex reaction; Frazer–Suzuki function; experimental and model plots

1 Introduction

The $M(II)HPO_4{\cdot}nH_2O$ [M(II)=Ca, Mg, Co, Mn, Ni, Zn, Cu; $0<n<3$] compounds with pores and acidity properties can be applied as catalysts, electric materials, conductors and ion exchangers [1]. With their calcined samples, $M_2P_2O_7$ compounds were used for wide applications [1]. In the recent work, $MnHPO_4{\cdot}3H_2O$ was used as a new precursor for the further generating of the cathode material $LiMnPO_4$ in Li-ion batteries [2]. The one-pot hydrothermal method was used to synthesize the thin-layered hydrate $CoHPO_4{\cdot}3H_2O$ for constructing the electrodes of supercapacitors [3]. In addition, the synthesis, kinetic parameters and thermodynamic functions of $MgHPO_4{\cdot}3H_2O$ were studied [1]. Many researchers synthesized the di-metal systems, $M_{1-x}A_xHPO_4{\cdot}nH_2O$ and $M_{2-2x}A_{2x}P_2O_7$, where A in the chemical formula is the 2nd metal(II) ion that improves their efficiency [4,5]. Nevertheless, the facile synthesis method with low cost and the analysis of the thermal property and the decomposition reaction of the tertiary-metal phosphate compound have received few attention. The thermal property analyses of the decompositions of the phosphate hydrates are important for changing the normal samples to the advanced materials [6]. In the previous studies, the metal-codoped cathode compounds, such as Fe-, Co-codoped $LiMn_{0.90}Fe_{0.05}Co_{0.05}PO_4$, Fe-, Mg-codoped $LiMn_{0.90}Fe_{0.05}Mg_{0.05}PO_4$, and Fe-, Zn-codoped $LiMn_{0.90}Fe_{0.05}Zn_{0.05}PO_4$, were generated to increase the electrochemical property of $LiMnPO_4$ [7]. The electrochemical performances of the above tertiary-metal compounds are higher than those of the single or binary-metal compounds [7]. Therefore, the authors attempted to generate the tertiary-metal compounds according to a simple, time-saving and inexpensive method. The synthesized samples were analyzed by the thermogravimetry (TG), differential thermogravimetry (DTG), differential thermal analysis (DTA), Fourier transform infrared (FTIR), scanning

Corresponding author: Chuchai SRONSRI; E-mail: chuchai_sronsri@hotmail.com
DOI: 10.1016/S1003-6326(18)64834-4

electron microscope (SEM), X-ray diffraction (XRD) and atomic absorption spectrophotometry (AAS) techniques. Considering the above $MnHPO_4·3H_2O$, $CoHPO_4·3H_2O$ and $MgHPO_4·3H_2O$ hydrate compounds, Co- and Mg-codoped $MnHPO_4·3H_2O$ or $Mn_{0.90}Co_{0.05}Mg_{0.05}PO_4·3H_2O$ compounds were selected to study in this work. The outcome is prospective to be useful in the evolution of the new precursors for the generation of the tertiary-metal cathode electrode materials ($LiMn_{0.90}Co_{0.05}Mg_{0.05}PO_4$) in Li-ion batteries with the improved properties in the future.

Certain solid-state reactions are complex with the overlapping processes [8]. Therefore, the investigation of the kinetic triplets including the activation energy E_α, pre-exponential factor A and kinetic model $f(\alpha)$ of single individual process is challenging. These kinetic parameters are determined for a perfect kinetic explanation of the total reaction process. The analytical procedures are applied for the measuring of the kinetic triplets of discrete processes. The analytical methods include model-free or isoconversional method [9], model-fitting procedure [10], master plots [11], nonparametric analysis [12] and combined kinetic analysis [13]. In general, the kinetic triplets are evaluated from TG data with the conversion factor (α) based on the recommendation of the Kinetics Committee of the International Confederation for Thermal Analysis and Calorimetry (ICTAC) for a single-step reaction [14]. The α values are calculated by the ratio of the mass loss from TG profiles. In this work, the investigation of the kinetic parameters was proposed and estimated from DTG data using an alternative calculation method. The α values can be calculated by the ratio of the peak area from DTG profiles followed by the analysis of the resulting deconvoluted curves to obtain the kinetic triplets. The confirmation will be tested by the comparison between the experimental and simulated curves. In the basic single kinetic step, the E_α value is unique and does not depend on α at any given time. The apparent E_α values were evaluated by an iterative integral isoconversional method. The reaction mechanism function was considered by comparing the experimental and model plots. Moreover, the A value was estimated from E_α and $f(\alpha)$. The corresponded standard thermodynamic functions (ΔS^Θ, ΔH^Θ and ΔG^Θ) of the transition-state (activated) complexes were computed from the kinetic triplets. The kinetic triplets and thermodynamic functions of the studied system as well as an alternative method to calculate the α values were determined, confirmed and reported for the first time in the present study.

2 Experimental

Tertiary-metal hydrate $Mn_{0.90}Co_{0.05}Mg_{0.05}HPO_4·3H_2O$ was generated by the straightway precipitation procedure. In a typical method, the 75 mL mixture solution of 25 mL of 0.45 mol/L $MnCl_2·4H_2O$, 25 mL of 0.025 mol/L $CoCl_2·6H_2O$ and 25 mL of 0.025 mol/L $MgCl_2·6H_2O$ was added to 25 mL of 0.5 mol/L H_3PO_4 solution with a mole ratio of 1:1 of the summation of all metals (Mn^{2+}+Co^{2+}+Mg^{2+}) to hydrogen phosphate (HPO_4^{2-}). The pH of the composition was adjusted to be about 7−8 by the summation of 1 mol/L NaOH (25 mL), and subsequently the pale pink precipitates were received. The obtained precipitates were sieved, and washed several times with deionized water (DI water) to remove the excess ions. Finally, the precipitates were dried in a desiccator for further observations. The preparation of the target compound was carried out according to the following reaction:

$$0.9Mn^{2+}+0.05Co^{2+}+0.05Mg^{2+}+HPO_4^{2-}+3H_2O \rightarrow Mn_{0.9}Co_{0.05}Mg_{0.05}HPO_4\cdot 3H_2O \quad (1)$$

The water contents in the synthesized crystalline hydrate were determined from the mass loss by the TG method on a Pyris Diamond instrument (Perkin–Elmer), whereas the divalent metal or M(II) contents were measured by the AAS method (Analyst 100, Perkin–Elmer). While, the FTIR spectra were scanned at room temperature in the wavenumber range of 4000− 370 cm^{-1} using the KBr pellet method (KBr with spectroscopy grade, Merck) on a Perkin–Elmer spectrum using the GX FTIR/FT Raman spectrophotometer with 40 scans and a resolution of 4 cm^{-1}. The structural investigation was operated at room temperature on a D8 advanced X-ray powder diffractometer (Bruker AXS) with Cu K_α radiation and 2θ range of 5°−70° with 0.02° increment, and scan speed of 1 s/step. The obtained XRD results were compared with the standard PDF database or Powder Diffraction File database of the ICDD or International Center for Diffraction Data. The obtained lattice parameters and cell volumes can be calculated from a least-squares refinement of the XRD file using a computer program that corrects systematic experimental errors. Furthermore, the crystallite size (D) can be evaluated using the equation of Scherrer as follows:

$$D=\frac{k\lambda}{\beta\cos\theta} \quad (2)$$

where k is a Scherrer constant taken as 0.89, which was widely used to compute the crystallite size of the particle from thermal solid-state process [15,16]. λ is 0.15406 Å (wavelength of the X-ray radiation), β is the full width at the half-maximum from the XRD intensity and θ is an experimental diffraction angle [17]. The SEM technique was used to study the morphologies after gold coating

using LEO SEM VP1450 model. The isoconversional or model-free kinetic study was operated from the resulted thermal solid-state reaction of DTG data at four different heating rates of 5, 10, 15 and 20 °C/min between 50 and 750 °C in air with a flow rate of 100 mL/min. About 8 mg sample was filling into an alumina pan (aluminum oxide or Al_2O_3, to protect the reaction between the selected pan and the studied material) without both lid and pressing. The calcined α-Al_2O_3 compound was used as the reference material in the experiment.

3 Theories

3.1 Deconvolution functions

The clearly seen alternative for the examination of complex procedures with overlapping reactions is the separation of the individual process by peak deconvolution using mathematic functions followed by the estimation of the separated (deconvoluted) peaks to evaluate the kinetic triplets. Various deconvolution techniques have been found in the literature, for example, thermal decomposition of polyurethane [18], wheat straw oxidative [19] and animal bones [20] were used for fitting complex reactions.

The objective of the present work was to use the four different deconvolution functions and to select the best fitting function for fitting the curve followed by the identification of the resulted individual curve to evaluate the kinetic triplets. Four different deconvolution functions were selected for the deconvolution process, namely

Gaussian:

$$y = a_0 \exp\left[-\frac{1}{2}\left(\frac{x-a_1}{a_2}\right)^2\right] \tag{3}$$

Lorentzian:

$$y = a_0\left[1+\left(\frac{x-a_1}{a_2}\right)^{-2}\right] \tag{4}$$

Weibull [21]:

$$y = a_0\left(\frac{a_3-1}{a_3}\right)^{(1-a_3)/a_3}\left[\frac{x-a_1}{a_2}+\left(\frac{a_3-1}{a_3}\right)^{1/a_3}\right]^{a_3-1}\cdot \exp\left\{-\left[\frac{x-a_1}{a_2}+\left(\frac{a_3-1}{a_3}\right)^{1/a_3}\right]^{a_3}+\frac{a_3-1}{a_3}\right\} \tag{5}$$

Frazer–Suzuki:

$$y = a_0 \exp\left\{-\ln 2\left[\left(\ln\left(1+2a_3\frac{x-a_1}{a_2}\right)\right)/a_3\right]^2\right\} \tag{6}$$

where the parameters a_0, a_1, a_2 and a_3 are the amplitude, position, half-width and asymmetry of the studied curve, respectively. After the best-fitting function was selected, the separated peaks were obtained and followed by kinetic analysis to evaluate the kinetic parameters.

3.2 Kinetic parameters

The reaction kinetics of the thermal decomposition of the crystalline compounds can be analyzed as the thermal solid-state reaction type [22,23]:

$$\text{A(solid)}\rightarrow\text{B(solid)}+\text{C(gas)} \tag{7}$$

In addition, the theory of solid-state decompositions for kinetics analysis was established [24−27]. The alternative approach to analyzing thermal decomposition kinetics is assigned to be

$$\text{A}_a\text{B}_b\text{(solid/liquid)}\rightleftharpoons a\text{A(gas)}+b\text{B(gas)}\rightarrow a\text{A(solid)}+b\text{B(gas)} \tag{8}$$

This process was described that a low-volatile product may be rapidly followed by condensation, a process in Eq. (8) promoted by the surface of a crystal of solid A [A(gas)→A(solid)].

In this work, the nonisothermal method was used to study the kinetic triplets using a model-free (isoconversional) method, which measures temperature (T) corresponding to the fixed value of the extent of conversion (α) at various heating rates (β):

$$\beta = \frac{\mathrm{d}T}{\mathrm{d}t} \tag{9}$$

where t is the time (min). In general, the α values from the thermogravimetric (TG) analysis are specified as the actual ratio of the mass loss corresponding to the investigated process:

$$\alpha = \frac{m_0 - m_t}{m_0 - m_\mathrm{f}} \tag{10}$$

where m_t is any mass of the sample at a time t, while m_0 and m_f are the masses of the sample at the starting point and end of the mass in the TG profile (tabular TG line), respectively.

In the present work, the α values can be calculated from the combined facile methods of the differential thermogravimetry (DTG) peak and Peak Analysis software. The α values were obtained from individual DTG peaks that were investigated after using the deconvolution technique (deconvoluted peak obtained from Peak Analysis software by a deconvolution function as discussed in Section 3.1), which were calculated by the ratio of the actual peak area corresponding to the investigated process as expressed in the following equation:

$$\alpha = \frac{S_T}{S_\mathrm{Total}} \tag{11}$$

where S_T is the resulted peak area at any temperature T and S_{Total} is the obtained total peak area calculated from an individual (deconvoluted) DTG peak that can be determined by combining DTG data and Peak Analysis software. In order to calculate the value of α, Eq. (11) was employed. The procedure is performed in the following three processes:

1) The overlapped DTG curve was analyzed and separated by suitable deconvolution function to obtain the deconvoluted DTG peak.

2) The separated DTG peak was used to evaluate the peak area.

3) The value of α can be calculated by the ratio between the peak area at the particular temperature T (S_T) and the total peak area (S_{Total}).

According to the isoconversional kinetic principle [22,23], the equation of the thermal decomposition kinetic from a solid-state reaction is considered to be based on the following equation:

$$\frac{\mathrm{d}\alpha}{\mathrm{d}t} = Af(\alpha)\exp\left(\frac{-E}{RT}\right) \tag{12}$$

Under nonisothermal status at a constant β, the rate is generally expressed as

$$\frac{\mathrm{d}\alpha}{\mathrm{d}t} \equiv \beta\frac{\mathrm{d}\alpha}{\mathrm{d}T} = Af(\alpha)\exp\left(\frac{-E}{RT}\right) \tag{13}$$

where A, E and $f(\alpha)$ are the kinetic parameters that are described in Section 1, while R is the mole gas constant.

According to Eq. (13), various procedures were developed to solve this equation. As shown by some analyses [28,29], the correct determination of the kinetic triplets involves the use of experimental file recorded for different values of β. These data used the isoconversional method in evaluation of E on α that can be related with the investigated reaction $f(\alpha)$. An isoconversional procedure is divided as either a linear or a nonlinear method. According to Eq. (13), both methods may be either differential or integral type. After integration of Eq. (13), Eq. (14) or its integral form of the reaction mechanism function $g(\alpha)$ was obtained as follows:

$$\int_0^{\alpha}\frac{\mathrm{d}\alpha}{f(\alpha)} \equiv g(\alpha) = \frac{A}{\beta}\int_0^{T_0}\exp\left(\frac{-E}{RT}\right)\mathrm{d}T \equiv \frac{A}{\beta}I(E_\alpha, T_\alpha) \tag{14}$$

where $g(\alpha)$ is the function in integral conversion form and $I(E_\alpha,T_\alpha)$ is the temperature integral form that cannot be resolved exactly because of the term $\int\exp(-x)$.

VYAZOVKIN [30] suggested a reformation of the integral nonlinear type [31] that determines $I(E_\alpha,T_\alpha)$ over the range of small $\Delta\alpha$ (modified nonlinear) to eliminate the systematic error. BUDRUGEAC [32] indicated that for $\Delta\alpha\to 0$ the E_α values obtained by this procedure are actually equal to those resulted by the Friedman method. CAI and CHEN [33] have suggested an iterative linear integral isoconversional method for the determination of E_α, which also uses the integration over the small $\Delta\alpha$ range and conduct to the correct or exact values of E_α in much less time than that suggested by Vyazovkin.

In this work, the iterative integral isoconversional equation with integration over a given range of the conversion α is used. This procedure has the following advantages: the applicability for the large and small $\Delta\alpha$ ranges, the probability of using precise estimations of $I(E_\alpha,T_\alpha)$, being applicable even when the original temperature corresponding to α=0 is randomly chosen from the range 0 to the minimum onset temperature, and the application in some favorable cases representing the α range in which the kinetics of the complicated investigated reaction is determined by a step characterized by E that does not depend on α.

The integration of Eq. (14) for the limits $\alpha_1(T_1)$ and $\alpha_2(T_2)$, and constant β leads to

$$g(\alpha_2) - g(\alpha_1) = \frac{A}{\beta}\int_{T_1}^{T_2}\exp\left(\frac{-E}{RT}\right)\mathrm{d}T \tag{15}$$

The integral linear isoconversional methods, such as KAS and OFW as well as the integral nonlinear isoconversional procedure suggested by VYAZOVKIN and DOLLIMORE [31] are considered when α_1=0. In such a condition [8],

$$\int_{T_0}^{T_1}\exp\left(\frac{-E}{RT}\right)\mathrm{d}T \approx 0 \tag{16}$$

and Eq. (15) turns into Eq. (14).

The integral temperature on the right-hand side [8] of Eq. (15) can be expressed as

$$I(E,T_1,T_2) = \int_{T_0}^{T_2}\exp\left(\frac{-E}{RT}\right)\mathrm{d}T - \int_{T_0}^{T_1}\exp\left(\frac{-E}{RT}\right)\mathrm{d}T \equiv \frac{E}{R}\left[p(x_2) - p(x_1)\right] \tag{17}$$

According to the numerous approximations, $p(x)$ is suggested and $x=E/(RT)$:

$$p(x) = \frac{\exp(-x)}{x}\pi(x) \tag{18}$$

Then, the eight-order approximation $\pi(x)$ [34] was used, which exhibits a very high accuracy:

$$\pi(x) = (x^7 + 70x^6 + 1886x^5 + 24920x^4 + 170136x^3 + 577584x^2 + 844560x + 357120)/(x^8 + 72x^7 + 2024x^6 + 28560x^5 + 216720x^4 + 880320x^3 + 1794240x^2 + 1572480x + 403200) \tag{19}$$

Therefore, Eq. (15) can be written as

$$g(\alpha_2)-g(\alpha_1)=\frac{AE}{R\beta}(T_2-T_1)\exp\left(\frac{-E}{RT_2}\right)\cdot \frac{p(x_2)-p(x_1)}{(T_2-T_1)\exp\left(\frac{-E}{RT_2}\right)} \tag{20}$$

from which the following equation is obtained as

$$\ln\frac{\beta}{(T_2-T_1)}=\ln\frac{A}{g(\alpha_2)-g(\alpha_1)}+\ln Q_T-\frac{E}{RT_2} \tag{21}$$

where

$$Q_T=\frac{\int_{T_1}^{T_2}\exp\left(\frac{-E}{RT_2}\right)\mathrm{d}T}{(T_2-T_1)\exp\left(\frac{-E}{RT_2}\right)}=\frac{E}{R}\frac{p(x_2)-p(x_1)}{(T_2-T_1)\exp\left(\frac{-E}{RT_2}\right)} \tag{22}$$

3.2.1 Activation energy E

In order to evaluate the E value, Eq. (21) was used. The following iterative procedure is applied in the following three steps:

1) Assume Q_T=1, and by plotting $\ln\frac{\beta}{(T_2-T_1)}$ versus $1/T_2$, E_1 is received from the slope of this straight line.

2) By introducing E_1 in the expression of Q_T, the value of E_2 is calculated from the slope of the straight line of $\ln\frac{\beta}{(T_2-T_1)}-\ln Q_T$ versus $1/T_2$.

3) Let E_2 replace E_1 and repeat step 2) until $|E_i-E_{i-1}|\le 0.1$ kJ/mol. The last E_i value will be considered to be the reliable apparent E_α value of the studied reaction.

In comparison with the bare integral isoconversional procedures (without iterative process) such as OFW and KAS methods, the mentioned iterative procedure (Eq. (22)) shows the superior advantage over the possibility of using $I(E_\alpha,T_\alpha)$ as one of the more precise estimations or the values of this integral to be exactly numerical. Another good point is that this method can be practical for all $\Delta\alpha$ ranges, even for the small $\Delta\alpha$ ranges.

3.2.2 Mechanism function determination

The Málek method [14,35] was used to select the suitable reaction mechanism function. According to the method, the especial function $z(\alpha)$ can be used for determination of the mechanism function. The temperature integral in Eq. (14) can be reformed as follows [14]:

$$g(\alpha)=\frac{AE_\alpha}{\beta R}\exp(-x)\frac{\pi(x)}{x} \tag{23}$$

Combining Eqs. (12) and (23) followed by some rearrangements allows one to express the $z(\alpha)$ function as follows:

$$z(\alpha)=f(\alpha)g(\alpha)=\left(\frac{\mathrm{d}\alpha}{\mathrm{d}t}\right)_\alpha T_\alpha^2\left[\frac{\pi(x)}{\beta T_\alpha}\right] \tag{24}$$

According to the heating rate β (Eq. (9)), Eq. (24) can be changed to Eq. (25) as follows:

$$z(\alpha)=f(\alpha)g(\alpha)=\beta\left(\frac{\mathrm{d}\alpha}{\mathrm{d}T}\right)_\alpha T_\alpha^2\left[\frac{\pi(x)}{\beta T_\alpha}\right] \tag{25}$$

According to the literatures [14,35], the term $\pi(x)/(\beta T_\alpha)$ in Eq. (25) has a slightly effect on the shape of the $z(\alpha)$ function. Thus, the shapes of $z(\alpha)$ can be determined for each α value by multiplying of the experimental values between $\beta(\mathrm{d}\alpha/\mathrm{d}T)_\alpha$ and T_α^2. The resulting experimental values of $z(\alpha)$ are plotted versus α and compared with the theoretical plots of $z(\alpha)$ that are received by plotting the product of $f(\alpha)g(\alpha)$ in Table 1 [8] versus α for several reaction models. Figure S1 [14] displays the theoretical plots of some $z(\alpha)$ functions for the models presented in Table 1. A suitable mechanism function is considered as the excellent matching between the experimental and theoretical (or model) plots. From a set of experimental kinetic curves measured for different heating rates, one can obtain a set of the experimental plots that, nevertheless, yield a single dependence of $z(\alpha)$ on α, which is practically independent of β. The above comparison procedure is an effective ways and recommended by the Kinetics Committee of the ICTAC [14].

3.2.3 Pre-exponential factor calculation

The pre–exponential factor magnitude in this work can be estimated by the basic equation of the method of Kissinger, and Eq. (12) was the second derivative expressed as follows:

$$\frac{\mathrm{d}}{\mathrm{d}t}\left(\frac{\mathrm{d}\alpha}{\mathrm{d}t}\right)=\frac{\mathrm{d}}{\mathrm{d}t}\left[Af(\alpha)\exp\left(\frac{-E}{RT}\right)\right] \tag{26}$$

From the second derivative, Eq. (26) can be expressed as

$$\frac{\mathrm{d}^2\alpha}{\mathrm{d}t^2}=A\left[f(\alpha)\frac{\mathrm{d}\exp(-E/RT)}{\mathrm{d}t}+\exp\left(\frac{-E}{RT}\right)\frac{\mathrm{d}f(\alpha)}{\mathrm{d}t}\right] \tag{27}$$

or

$$\frac{\mathrm{d}^2\alpha}{\mathrm{d}t^2}=A\left[f(\alpha)\exp\left(\frac{-E}{RT}\right)\frac{\mathrm{d}(-E/RT)}{\mathrm{d}t}+\exp\left(\frac{-E}{RT}\right)f'(\alpha)\frac{\mathrm{d}\alpha}{\mathrm{d}t}\right] \tag{28}$$

where

$$f'(\alpha)=\frac{\mathrm{d}f(\alpha)}{\mathrm{d}\alpha} \tag{29}$$

Table 1 $f(\alpha)$, $f'(\alpha)$ and $g(\alpha)$ functions for most widely-used kinetic models

Kinetic model	Code	$f(\alpha)$	$f'(\alpha)$	$g(\alpha)$
Phase boundary controlled reaction (contracting area)	R_2	$2(1-\alpha)^{1/2}$	$\frac{-1}{(1-\alpha)^{1/2}}$	$1-(1-\alpha)^{1/2}$
Phase boundary controlled reaction (contracting volume)	R_3	$3(1-\alpha)^{2/3}$	$\frac{-2}{(1-\alpha)^{1/3}}$	$1-(1-\alpha)^{1/3}$
Random nucleation followed by an instantaneous growth of nuclei (Avrami–Erofeev, n=1)	F_1	$1-\alpha$	-1	$-\ln(1-\alpha)$
Random nucleation and growth of nuclei through different nucleation and nucleus growth models (Avrami–Erofeev, $n\neq1$)	A_n	$(1-\alpha)[-\ln(1-\alpha)]^{1-1/n}$	$n+n\ln(1-\alpha)-\frac{1}{[-\ln(1-\alpha)]^{1/n}}$	$[-\ln(1-\alpha)]^{1/n}$
2D diffusion	D_2	$\frac{1}{[-\ln(1-\alpha)]}$	$\frac{-1}{(1-\alpha)[\ln(1-\alpha)]^2}$	$\alpha+(1-\alpha)\ln(1-\alpha)$
3D diffusion (Jander)	D_3	$\frac{3(1-\alpha)^{2/3}}{2[1-(1-\alpha)^{1/3}]}$	$\frac{\frac{1}{2}-(1-\alpha)^{-1/3}}{[1-(1-\alpha)^{1/3}]^2}$	$[1-(1-\alpha)^{1/3}]^2$
3D diffusion (Ginstling–Brounshtein)	D_4	$\frac{3}{2}[(1-\alpha)^{1/3}-1]$	$\frac{-(1-\alpha)^{4/3}}{2[(1-\alpha)^{-1/3}-1]^2}$	$1-2/3\alpha-(1-\alpha)^{2/3}$

$f'(\alpha)$ can be rewritten as $\frac{\mathrm{d}f(\alpha)}{\mathrm{d}t}\frac{\mathrm{d}\alpha}{\mathrm{d}\alpha}$ and leads to Eq. (28). Subsequently, Eq. (30) is obtained as follows:

$$\frac{\mathrm{d}^2\alpha}{\mathrm{d}t^2}=\frac{\beta E}{RT^2}\frac{\mathrm{d}\alpha}{\mathrm{d}t}+A\exp\left(\frac{-E}{RT}\right)f'(\alpha)\frac{\mathrm{d}\alpha}{\mathrm{d}t} \tag{30}$$

At the maximum reaction rate status, the second derivative of $\frac{\mathrm{d}\alpha}{\mathrm{d}\alpha}$ or $\frac{\mathrm{d}^2\alpha}{\mathrm{d}t^2}$ of Eq. (30) is 0:

$$\frac{\mathrm{d}^2\alpha}{\mathrm{d}t^2}=\left[\frac{\beta E}{RT_{\max}^2}+Af'(\alpha_{\max})\exp\left(\frac{-E}{RT_{\max}}\right)\right]\left(\frac{\mathrm{d}\alpha}{\mathrm{d}t}\right)_{\max}=0 \tag{31}$$

where the subscript "max" indicates the value implicated to the highest or the maximum of the temperature obtained from the result of individual DTG peak at a β of 5 °C/min. Note that the first derivative of the conversion $(\mathrm{d}\alpha/\mathrm{d}t)_{\max}$ is not equal to 0. Therefore, as a result of Eq. (31), the following equation is obtained:

$$\frac{\beta E}{RT_{\max}^2}+Af'(\alpha_{\max})\exp\left(\frac{-E}{RT_{\max}}\right)=0 \tag{32}$$

After the rearrangement of Eq. (32), the values of the pre-exponential factor A can be calculated according to Eq. (33) [14,36] as follows:

$$A=\frac{-\beta E}{RT_{\max}^2 f'(\alpha_{\max})}\exp\left(\frac{E}{RT_{\max}}\right) \tag{33}$$

4 Results and discussion

4.1 Characterization

Experimental TG and DTA curves at a β of 5 °C/min from the solid-state reaction of the synthesized compound $Mn_{0.90}Co_{0.05}Mg_{0.05}HPO_4{\cdot}3H_2O$ are shown in Fig. 1. The thermal solid-state reaction takes place in two steps in the temperature range of 50−750 °C. The mass loss starts at ~85 °C and ends up at ~630 °C. According to the TG result at β of 5 °C/min, the obtained total mass loss is 32.46%, which is in good acceptance with the theoretical data of 32.56%. The mass loss of the first (85−200 °C) and final (200−630 °C) steps were 26.49% and 5.97%, respectively, which guarantees very good agreement with the theoretical data of 26.54% and 6.02%, respectively. In addition, the four corresponding DTG curves at four different heating rates of 5, 10, 15 and 20 °C/min are displayed in Fig. 2. The obvious DTG peak profile with the shoulder in the first step in Fig. 2 corresponds to the elimination of water (H_2O) molecules or the dehydration process from the synthesized crystalline hydrate to form an amorphous phase $Mn_{0.90}Co_{0.05}Mg_{0.05}HPO_4$, which demonstrates two different strengths in H bonding of H_2O molecules in the structure of hydrate crystal. The complicated overlapping in the DTG peak of the first thermal decomposition step agrees with the result of its related samples, single-metal $MnHPO_4{\cdot}3H_2O$ [2] and binary-metal $Mn_{0.90}Co_{0.1}HPO_4{\cdot}$

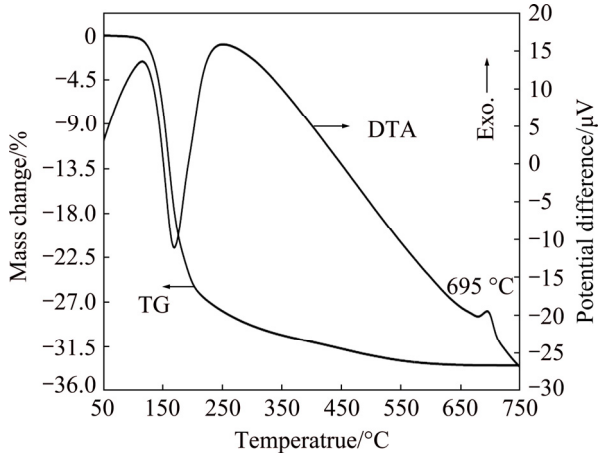

Fig. 1 Thermal solid-state reaction process of synthesized hydrate compound $Mn_{0.90}Co_{0.05}Mg_{0.05}HPO_4{\cdot}3H_2O$ demonstrated as TG and DTA curves in temperature range of 50−750 °C at heating rate of 5 °C/min under atmosphere of air with flow rate of 100 mL/min

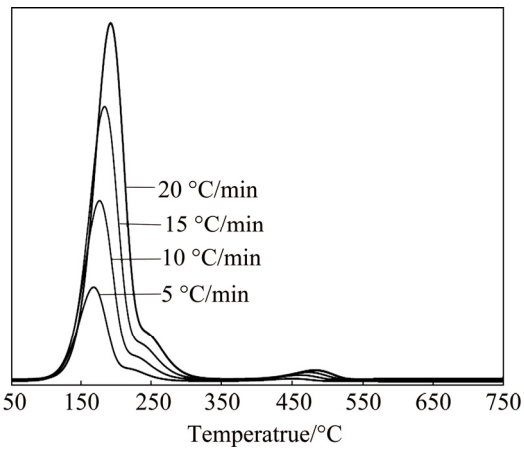

Fig. 2 DTG curves of thermal solid-state reaction processes in temperature range of 50−750 °C at different heating rates of 5, 10, 15 and 20 °C/min under atmosphere of air with flow rate of 100 mL/min of synthesized hydrate compound $Mn_{0.90}Co_{0.05}$-$Mg_{0.05}HPO_4{\cdot}3H_2O$

$3H_2O$ [34] compounds. Moreover, the final step coincides with the dehydration of the water constituent from the HPO_4^{2-} group or the polycondensation to form an amorphous phase $Mn_{1.8}Co_{0.1}Mg_{0.1}P_2O_7$. In addition, the obvious exothermic DTA peak profile at about 695 °C of β=5 °C/min in Fig. 1 can be summarized as the phase change or phase transition from low crystalline sample (an amorphous) $Mn_{1.8}Co_{0.1}Mg_{0.1}P_2O_7$ to the crystalline monoclinic phase $Mn_{1.8}Co_{0.1}Mg_{0.1}P_2O_7$. According to the results from the TG/DTG/DTA solid-state reaction curves, two thermal reaction steps of the synthesized hydrate $Mn_{0.90}Co_{0.05}Mg_{0.05}HPO_4{\cdot}3H_2O$ are suggested as follows:

First step (85−200 °C), dehydration:

$$Mn_{0.90}Co_{0.05}Mg_{0.05}HPO_4{\cdot}3H_2O(s)\rightarrow Mn_{0.90}Co_{0.05}Mg_{0.05}HPO_4(s)+3H_2O(g) \quad (34)$$

Final step (200−630 °C), polycondensation (H_2O elimination from the constituent of HPO_4^{2-} group):

$$Mn_{0.90}Co_{0.05}Mg_{0.05}HPO_4(s)\rightarrow 0.5Mn_{1.8}Co_{0.1}Mg_{0.1}P_2O_7(s)+0.5H_2O(g) \quad (35)$$

Figure S2 demonstrates the resulted FTIR spectra of the synthesized hydrate $Mn_{0.90}Co_{0.05}Mg_{0.05}HPO_4{\cdot}3H_2O$ and its thermal solid-state reaction product $Mn_{1.8}Co_{0.1}Mg_{0.1}P_2O_7$. The vibrational spectrum of the synthesized hydrate in Fig. S2(a) is very similar to that of $MgHPO_4{\cdot}3H_2O$ [1], $MnHPO_4{\cdot}3H_2O$ [2] and $Mn_{0.9}Co_{0.1}$-$HPO_4{\cdot}3H_2O$ [34]. It can be seen from the spectrum of the synthesized hydrate that the broad band positions in the wavenumber range of 3600−3100 cm^{-1} with two position peaks at 3513 and 3276 cm^{-1} in Fig. S2(a) are assigned to the O—H asymmetric $\nu_3B_2(H_2O)$ and symmetric $\nu_1A_1(H_2O)$ stretching vibration modes, respectively. On the other hand, the two broad band positions observed in the wavenumber range of 1820−1570 cm^{-1} are specified to two different H_2O bending modes $\nu_2A_1(H_2O)$ at 1704 and 1656 cm^{-1} at two various crystallographic sites and two different hydrogen bond intensities of the synthesized crystalline hydrate. This result is in agreement with its DTG curve and the results from the literatures [2,34], which indicates that the water molecules are eliminated at two main temperatures. In typical descriptions of the vibrational spectra of the HPO_4^{2-} unit, the spectra are observed in the wavenumber range of 3030−2720 cm^{-1} (with the observed maximum peak at 2930 cm^{-1}) and 2570−2270 cm^{-1} (two peaks at 2478 and 2406 cm^{-1}), which are assigned to the asymmetric stretching $\nu_{OH}(HPO_4^{2-})$ and symmetric stretching $\nu_{OH}(HPO_4^{2-})$, respectively. Furthermore, the vibrational spectra are obtained in the region of 1320−1128 cm^{-1} (two peaks at 1247 and 1171 cm^{-1}), 1132−944 cm^{-1} (two peaks at 1064 and 1017 cm^{-1}), 945−842 cm^{-1} (a peak at 893 cm^{-1}), 840−584 cm^{-1} (a peak at 692 cm^{-1}) and 584−440 cm^{-1} (a peak at 516 cm^{-1}), and these modes are assigned to $\nu(PO_3)$, $\delta(POH)$, $\nu(PO_2(OH))$, $\gamma(POH)$ and $\delta(PO_3)$, respectively [1,2,34]. The water band positions at 3513, 3276, 1704 and 1656 cm^{-1} disappear after the combustion process, which shows the dehydration process of the synthesized $Mn_{0.90}Co_{0.05}Mg_{0.05}HPO_4{\cdot}3H_2O$ to form amorphous $Mn_{0.90}Co_{0.05}Mg_{0.05}HPO_4$. On the contrary, the calcined sample at 630 °C in Fig. S2(b) shows the characteristic peaks of $Mn_{1.8}Co_{0.1}Mg_{0.1}P_2O_7$ according to the polycondensation process or the elimination of the water molecule from the constituent of HPO_4^{2-} unit [1,2,34]. The FTIR bands are analyzed based on the basic vibrating unit of the $P_2O_7^{4-}$ anion

group. The vibrational modes include the asymmetric PO_2 ($v_{asym}(PO_2)$) and symmetric PO_2 ($v_{sym}(PO_2)$) stretching modes observed around 1250−955, 1245−1145 and 1155−1015 cm^{-1} regions, respectively. On the other hand, the asymmetric v_{asym}(O—P—O) and the symmetric v_{sym}(O — P — O) bridge modes are outstanding in the 1010−945 and 765−405 cm^{-1} regions, respectively.

The XRD patterns of the prepared hydrate compound and its complete thermal solid-state reaction compound are represented in Fig. S3. The smooth baseline and excellent intensity of the resulted diffraction pattern show the good crystallinity of both compound of hydrate and its final decomposition product. According to Fig. S3(a), all resulted XRD pattern peaks are obviously confirmed as the orthorhombic crystal system of the $Mn_{0.90}Co_{0.05}Mg_{0.05}HPO_4{\cdot}3H_2O$ sample with the space group *Pbca* (No. 61) and the standard lattice parameters are found to be a=10.400 Å, b=10.860 Å and c=10.192 Å by comparison with the PDF number 79–0730 of the $MnHPO_4{\cdot}3H_2O$ sample database. In this work, the calculated cell parameters are found to be a=10.420 Å, b=10.844 Å and c=10.201 Å with $\alpha=\beta=\gamma=90°$, which are in good agreement with the above standard data. Apart from that, the corresponding obtained cell volume and crystallite size are 1152.66 $Å^3$ (obtained from the multiple product of $abc\sin\beta$) and 49.8 nm, respectively. On the other hand, the diffraction data of the good-crystalline monoclinic phase of the $Mn_{1.8}Co_{0.1}Mg_{0.1}P_2O_7$ sample in Fig. S3(b) are obviously observed after the complete thermal solid-state reaction processes of its synthesized hydrate, which can be confirmed with the standard data by $Mn_2P_2O_7$ sample database according to PDF number 77−1243 with the monoclinic crystal system and space group $C2/m$ (No. 12). While, the lattice parameters are found to be a=6.633 Å, b=8.584 Å and c=4.646 Å. The calculated cell lattice or cell parameters in this work are found to be a=6.631 Å, b=8.580 Å and c=4.649 Å, and $\alpha=\gamma=90°\neq\beta=102.24°$, which are in good agreement with the above standard data. The corresponding calculated cell volume in this work is 260.99 $Å^3$ (obtained from the product of $abc\sin\beta$), while the crystallite size is 44.5 nm. The resulted XRD patterns of the hydrate compound $Mn_{0.90}Co_{0.05}Mg_{0.05}HPO_4{\cdot}3H_2O$ and its final thermal solid-state reaction product $Mn_{1.8}Co_{0.1}Mg_{0.1}P_2O_7$ are in excellent agreement with those of the single-metal $MnHPO_4{\cdot}3H_2O$ [2] and binary-metal $Mn_{0.9}Co_{0.1}HPO_4{\cdot}3H_2O$ [34] compounds. In addition, the XRD pattern of $LiMn_{0.90}Co_{0.05}Mg_{0.05}PO_4$ is shown in Fig. S3(c). This diffraction pattern was obtained from the thermal solid-state reaction of the solid mixture between the synthesized $Mn_{0.90}Co_{0.05}Mg_{0.05}HPO_4{\cdot}3H_2O$ and a Li-source of Li_2CO_3 according to the Refs. [2,6]. In typical preparation of $LiMn_{0.90}Co_{0.05}Mg_{0.05}PO_4$ compound, the stoichiometric mole ratio between $Mn_{0.90}Co_{0.05}Mg_{0.05}HPO_4{\cdot}3H_2O$ and Li_2CO_3 of 2:1 was finely ground by hand in a mortar for about 45 min to complete the homogeneous composition. After the calcination of the mixture at 800 °C [2], $LiMn_{0.90}Co_{0.05}Mg_{0.05}PO_4$ was obtained and washed several times with DI water to remove the excess ions (unreacted ions), dried at 110 °C for one night (about 12 h). Therefore, the tertiary-metal cathode material $LiMn_{0.90}Co_{0.05}Mg_{0.05}PO_4$ can be synthesized from the tertiary-metal phosphate compound $Mn_{0.90}Co_{0.05}Mg_{0.05}HPO_4{\cdot}3H_2O$.

The SEM micrographs of synthesized hydrate and anhydrase compounds ($Mn_{0.90}Co_{0.05}Mg_{0.05}HPO_4{\cdot}3H_2O$ and $Mn_{1.8}Co_{0.1}Mg_{0.1}P_2O_7$) are shown in Fig. S4. Figure S4(a) displays the irregular plate-like shape of the hydrate form with the sizes of about 4−6 μm in width, 5−9 μm in length and 0.3−0.9 μm in thickness with the tiny plates of about 1−3 μm. In contrast, the morphologies of the anhydrous form in Fig. S4(b) show irregular shape with different sizes of about 1−6 μm in width. The morphologies of the anhydrous compound are different from those of the hydrate compound, which is caused by the whole solid-state reaction in the sequence of dehydration, polycondensation and crystallization processes, respectively.

The metal amounts of Mn, Co and Mg metals per chemical formula of the obtained hydrate compound and its final thermal solid-state reaction product were determined by the AAS method. The results show that the amounts of the above three metals are 0.892, 0.049 and 0.051 mole per chemical formula of the studied hydrate sample, respectively. However, the mole ratio of Mn:Co:Mg metals from the synthesis part is 0.90:0.05:0.05. According to the AAS results and the synthesis part, the chemical formula of the studied compound is fixed as 0.90 Mn, 0.05 Co and 0.05 Mg, respectively. On the other hand, the amount of water of 2.98 mol per chemical formula of the synthesized hydrate compound was calculated by the mass loss from TG data. The results from these methods together with the FTIR spectra (characteristic IR peaks of the hydrogen phosphate anion HPO_4^{2-} and the H_2O unit) and XRD patterns (compared with the standard target PDF numbers) confirm that the chemical formula of the synthesized hydrate compound is $Mn_{0.90}Co_{0.05}Mg_{0.05}HPO_4{\cdot}3H_2O$, whereas its thermal solid-state reaction product is $Mn_{1.8}Co_{0.1}Mg_{0.1}P_2O_7$ sample.

4.2 Kinetics and thermodynamics results

4.2.1 Apparent E_α values

DTG profiles at different heating rates (β) of 5, 10, 15 and 20 °C/min under nonisothermal solid-state reaction conditions of the hydrate compound are

displayed in Fig. 2. The observed temperature T of the resulted DTG peaks increases with an increase in the β to equalize the reduction of time t [34]. If the E_α values are stable over the α range and multiple peaks or shoulders are not found in the resulted thermal solid-state reaction curve such as DTG result, it is probable that the process is considered as a single-step of kinetic reaction and can be sufficiently explained by a kinetic single-step process [14]. Moreover, it is increasingly regular that the E_α values vary importantly with the α. If the resulted reaction curve (DTG) has the shoulders and/or multiple peaks, the E_α values at suitable levels of α can be applied as input to fitting mathematics of the multi-step model [14]. Furthermore, it can also be discussed as the kinetic single-step process, if the calculated E_α values are free of α so that the change values of the maximum E_α or minimum E_α values from the average E_α must be less than 10% [14]. The calculated differences are also considered to confirm the kinetic single-step process of the studied thermal solid-state reaction process.

According to the DTG curves in Fig. 2, the peaks have the shoulders and/or multiple peaks. Therefore, the deconvolution function was used to separate the subpeak in the overlapping area for further characterization. According to Section 3.1, the Gaussian and Lorentzian equations are symmetric and basically rule out most real-life kinetic models [8]. Therefore, the analyses of the kinetic results of the individual process obtained from the Gaussian and Lorentzian deconvolution functions are fundamentally incorrect and lead to highly biased and false results [8]. For proper deconvoluted models that allow asymmetry need to be considered. After applying the deconvolution technique of four fitting functions, the suitable results with Lorentzian (symmetry profile), Gaussian (symmetry profile) and Weibull (asymmetry profile) functions had poor fitting results, whereas the Frazer–Suzuki (asymmetry profile) equation nicely fitted the kinetic reaction result of DTG curve. After using the deconvolution method of the suitable Frazer–Suzuki fitting function, three individual DTG peaks at β of 5 °C/min were obtained and shown in Fig. 3. Figure S5 illustrates three individual DTG peaks with their peak areas at β of 5 °C/min, which is used to calculate the α values. After obtaining the peak area from each deconvoluted DTG peak, the α values were calculated by the ratio between the peak area at the specific temperature T (S_T) and the total peak area (S_{Total}) from Eq. (11). The relations between the α or dα/dt values and temperature T of three thermal solid-state reaction processes are shown in Fig. 4. The maximum DTG temperatures $T_{\max}$ obtained from the highest kinetic rate for individual peaks are 440.86 K (167.71 °C), 489.75 K (216.60 °C) and 723.10 K (449.95 °C) with the corresponding α values of 0.56, 0.59 and 0.63 (α≠0.50, asymmetric curves), respectively.

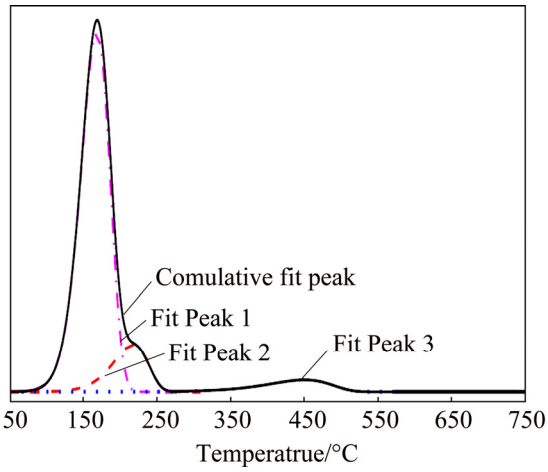

Fig. 3 Deconvoluted DTG peaks observed from overlapped DTG curve of thermal solid-state reaction processes of synthesized hydrate compound $Mn_{0.90}Co_{0.05}Mg_{0.05}HPO_4{\cdot}3H_2O$ in temperature range of 50−750 °C at heating rate (β) of 5 °C/min

The iterative integral isoconversional equation (Eq. (21)) was used to calculate the apparent E_α values of three individual peaks corresponding to the various α values in the range of 0.10−0.90 (with an increment of 0.02). The variation of E_α and A for α<0.1 and α>0.90 is not a major concern generally because these parameters can be importantly affected by probable minor errors in the baseline determination [14]. The relations between E_α and α of the separated DTG peaks obtained from the iterative integral isoconversional equation are shown in Fig. 5. In the present work, the average apparent E_α values of the individual thermal solid-state reaction processes were calculated from the iterative equation plots and found to be (65.87±2.95), (78.16±3.74) and (119.32±5.81) kJ/mol with the corresponding average r^2 (correlation coefficient from the straight lines) of 0.9987, 0.9995 and 0.9991, respectively. Moreover, the E_α values of all individual peaks were slightly changed with the increase in α. In addition, the E_α values of the second individual peak were higher than those of the first individual peak. It can be due to the two groups of water of the synthesized hydrate crystal structure, which have different hydrogen bonds (H-bonds). The H-bond from the first individual peak is the week reaction. On the other hand, the H-bond from the second individual peak is the strong reaction and can affect the stability of the structure and hence increase the energy in order to break the water from the structure of the dehydration process. These results are in agreement with the shoulders observed in TG, DTG and DTA plots and two bands of the H_2O bending mode in FTIR techniques. The calculated E_α values from the thermal decomposition of the solid-state reaction of the resulted hydrate are

discovered to increase in the sequence of the first, second and final individual peaks. It can be seen from Fig. 5 that the E_α–α relation curves in the first and second individual peaks correspond to the dehydration reaction processes.

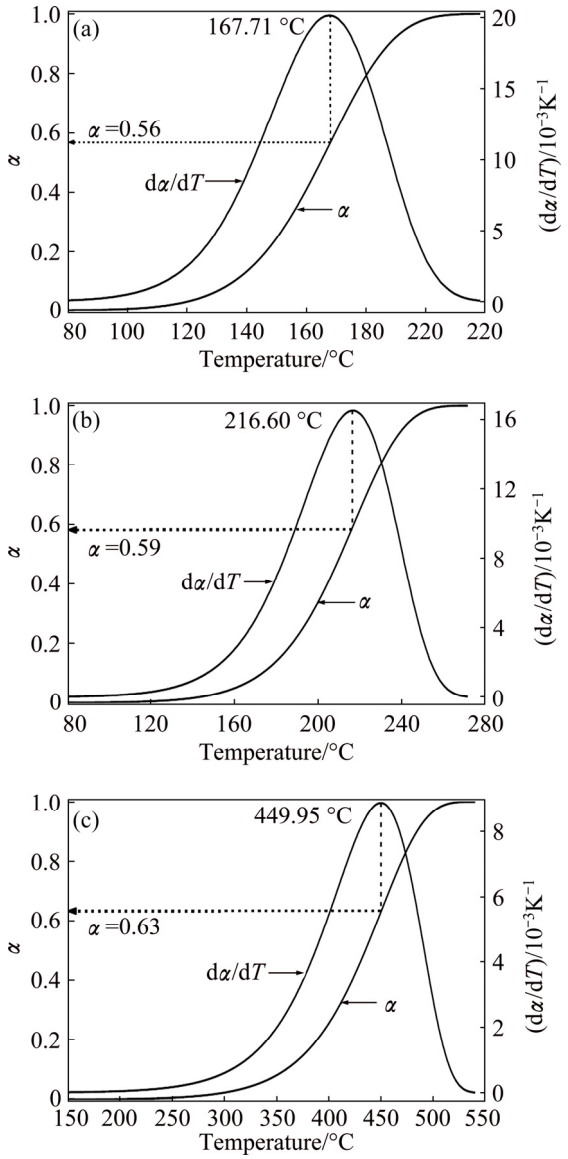

Fig. 4 Relation between α or dα/dT and T obtained from first (167.71 °C) (a), second (216.60 °C) (b) and final (449.95 °C) (c) individual peaks with highest dα/dT observed from deconvoluted peak of thermal solid-state reaction processes of $Mn_{0.90}Co_{0.05}Mg_{0.05}HPO_4{\cdot}3H_2O$ in temperature range of 50−750 °C at heating rate (β) of 5 °C/min

According to Figs. S2, 2, 3 and 5, it is obvious that the thermal solid-state reaction of the dehydration process is a kinetically complex reaction and cannot be discussed as a single-step reaction. However, the reaction curve or the DTG peak could be separated as an individual peak and concluded as a single-step process, and each individual peak can be treated by the unique kinetic parameters [2]. The relative errors between the

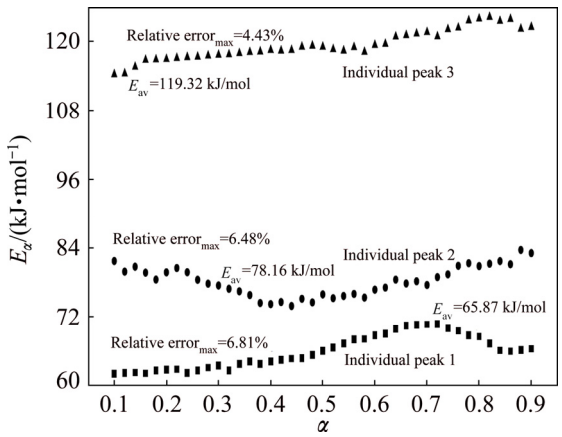

Fig. 5 Relation between E_α and α including relative error for first (6.81%), second (6.48%) and final (4.43%) individual peaks (less than 10% of average E_α values indicating single-step process) of thermal solid-state reaction processes of $Mn_{0.90}Co_{0.05}Mg_{0.05}HPO_4{\cdot}3H_2O$

maximum of E_α values and the average of E_α values of the first, second and final individual peaks are shown in Fig. 5. The resulted maximum relative errors are 6.81%, 6.48% and 4.43%, respectively. These values are less than 10% of the average E_α values. For this reason, the first, second and final individual peaks were concluded to be the single-step system of the kinetic reaction and can be completely explained by the unique kinetic parameters. In addition, in order to calculate the amounts of water from the first and second individual peaks, the peak area of the first and second individual peaks were used. The amount of water can be calculated from the ratio between each peak area and the summation of the two individual peaks. According to Fig. S5, the peak area of the first peak is 45080, whereas that of the second peak is 6173. Therefore, the amounts of water calculated from the areas of the first and second peaks are about 2.5 and 0.5 mol, respectively. The relation between the water contents and FTIR results can be described that the water amount of 0.5 mol was last eliminated because of strong bond. This result corresponded with the FTIR position peak at 1704 cm^{-1} (higher energy). On the other hand, the FTIR position peak at 1656 cm^{-1} (lower energy) was described in contrast corresponding to the water amount of 2.5 mol. According to the reported results of the amount of water as well as the results from Figs. S2, 2, 3, S5 and 5, only first thermal solid-state reaction process of the synthesized $Mn_{0.90}Co_{0.05}Mg_{0.05}HPO_4{\cdot}3H_2O$ compound is suggested and expressed as follows:

1) Individual peak 1 (single-step process), dehydration I process:

$$Mn_{0.90}Co_{0.05}Mg_{0.05}HPO_4{\cdot}3H_2O(s)\rightarrow Mn_{0.90}Co_{0.05}Mg_{0.05}HPO_4{\cdot}0.5H_2O(s)+2.5H_2O(g) \quad (36)$$

2) Individual peak 2 (single-step process), dehydration II process:

$$Mn_{0.90}Co_{0.05}Mg_{0.05}HPO_4\cdot 0.5H_2O(s)\rightarrow Mn_{0.90}Co_{0.05}Mg_{0.05}HPO_4(s)+0.5H_2O(g) \quad (37)$$

Whereas the individual peak 3 (single-step process) is the elimination of water constituent from the hydrogen phosphate or the polycondensation process as expressed in Eq. (35).

4.2.2 Obtained reaction mechanism function

According to the nonisothermal condition, experimental information and the calculated values of the apparent E_α calculated from the iterative integral isoconversional method in Eq. (21) (model-free method), the variation of $d\alpha/dT$ versus T at β=5 °C/min for all thermal solid-state reactions includes the first, second and final individual peaks of the synthesized $Mn_{0.90}Co_{0.05}Mg_{0.05}HPO_4\cdot 3H_2O$ hydrate, as shown in Figs. 4(a), (b) and (c), respectively. Then, the mentioned Málek method in Eq. (25) is used to create the plots of the experimental data between the normalized $z(\alpha)$ versus α at β=5 °C/min. The resulted experimental plots show insignificant difference along with the other three β values (10, 15 and 20 °C/min) [14]. After that, the suitable reaction mechanisms for all thermal solid-state reaction processes are determined and considered by comparison between the experimental against reaction model (theoretical) plots. The theoretical reaction model plots are clearly obtained from Table 1 by multiplying $f(\alpha)$ and $g(\alpha)$ equations to obtain $z(\alpha)$ by inserting the α values from 0 to 1 with 0.02 of an increment in each reaction model. Figure 6 shows the variation of the true

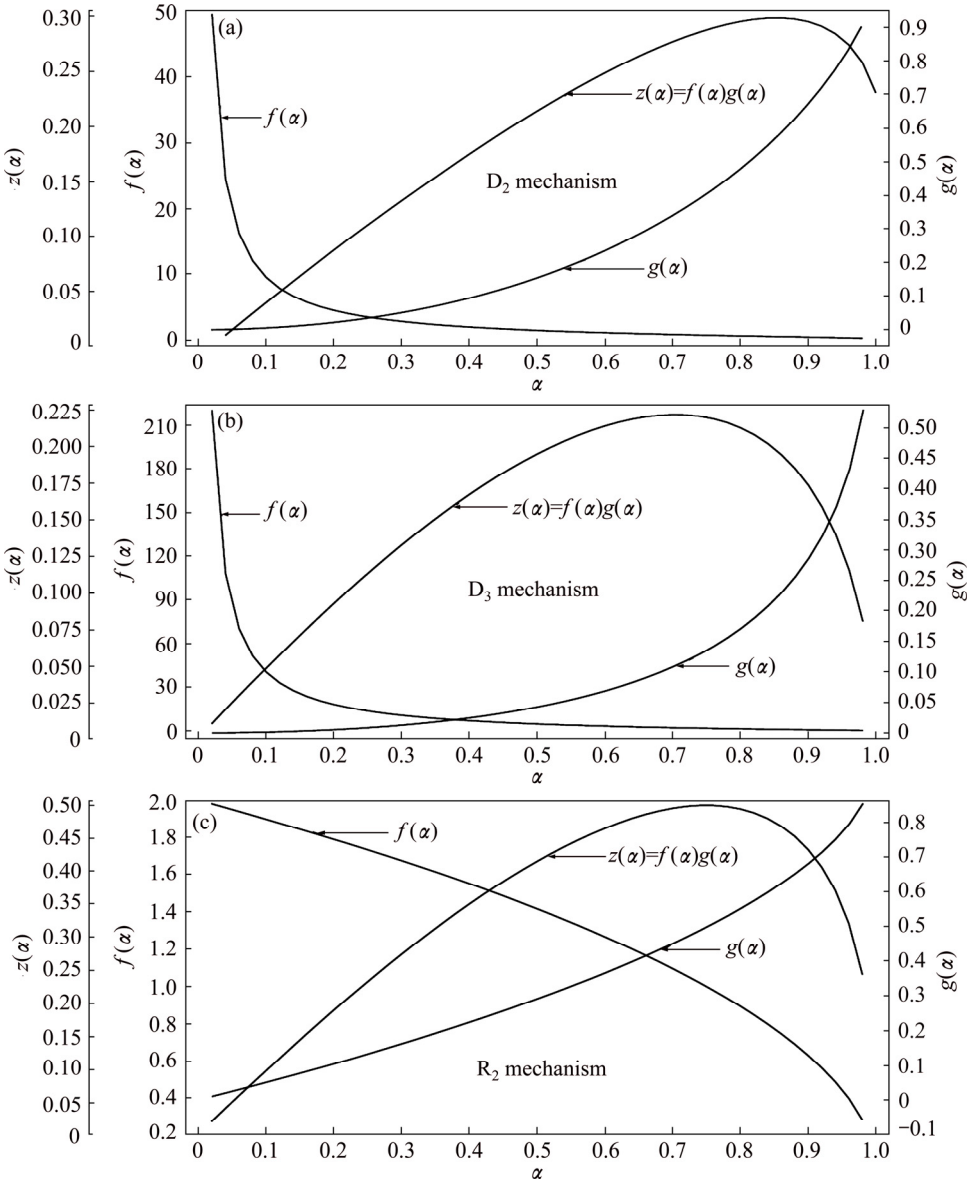

Fig. 6 Variation of truth values without normalization of $f(\alpha)$, $g(\alpha)$, $z(\alpha)$ against corresponding α values for first (a), second (b) and final (c) individual peaks of thermal solid-state reaction processes of synthesized hydrate compound $Mn_{0.90}Co_{0.05}Mg_{0.05}HPO_4\cdot 3H_2O$ in temperature range of 50−750 °C at heating rate (β) of 5 °C/min

values without the normalization of $f(\alpha)$, $g(\alpha)$ and $z(\alpha)$ against the corresponding α values for the first, second and final individual peaks. On the other hand, the relations between the normalized $z(\alpha)$ and α values of each individual peak are illustrated in Fig. 7. According to the comparison results, the best reaction mechanism functions for the studied first, second and final individual peaks are determined and the excellent matching reaction functions are found to be D_2, D_3 and R_2, respectively. The mechanism functions of the first and second individual peaks are the diffusion mechanism, whereas the mechanism function of the final individual peak is based on the deceleratory rate equation of the type of the phase boundary controlled reaction. These results show that the sequence of the thermal reaction processes are forced by the solid-state reaction processes characterized by the 2D (two-dimensional diffusion, D_2), 3D (three-dimensional diffusion, D_3) and contracting cylinder (cylindrical symmetry, R_2), respectively. According to the obtained results, it can be concluded that the dehydration reaction in the first and second individual peaks of the thermal solid–state reaction processes occurred as two consecutive reaction mechanism functions. For the first elimination reaction, 2.5 mol of water amount of the crystallized hydrate compound was eliminated by the two-dimensional diffusion (D_2) mechanism reaction function, whereas the second elimination reaction of 0.5 mol of water amount was eliminated by the three-dimensional diffusion (D_3) function. These results were in agreement with the observation of the FTIR result of different H-bonds of two groups in the bending mode (1704 and 1656 cm^{-1}) of water in the crystallized hydrate compound. In addition, the obtained results were also in agreement with the overlapped peak in the DTG curve.

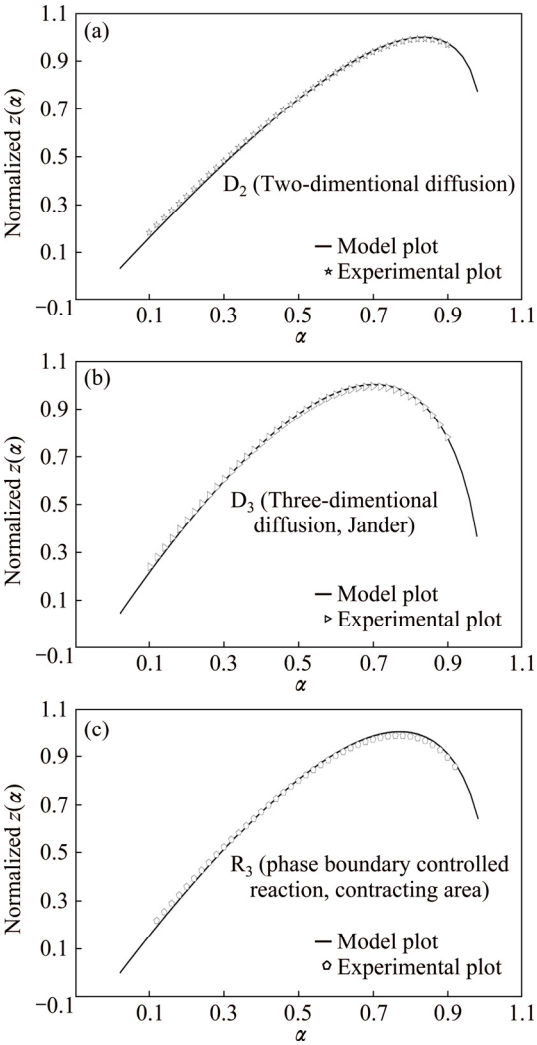

Fig. 7 Experimental and model plots with excellent matching results obtained from plots between normalized $z(\alpha)$ and α values of three thermal solid-state reaction processes at heating rate of 5 °C/min: (a) First step, dehydration I; (b) Second step, dehydration II; (c) Final step, polycondensation

4.2.3 Pre-exponential factor

The frequency factor or pre–exponential factor (A) values of the thermal solid-state reaction processes of the studied hydrate were calculated using Eq. (33) after receiving the suitable reaction mechanism function as described in Section 4.2.2. All calculated parameters are substituted into Eq. (33) at β=5 °C/min, and then the activation energies E_α of (65.87±2.95) and (78.16±3.74) kJ/mol and reaction mechanisms D_2 and D_3 were obtained from the dehydration I and II for individual peak 1 and 2, respectively. On the other hand, the final individual peak provides the values of (119.32±5.89) kJ/mol for E_α and the reaction mechanism is R_2. The maximum DTG temperatures (T_{max} related to the highest kinetic rate) for the individual peaks 1, 2, and 3 are found to be 440.86, 489.75 and 723.10 K with the corresponding α values of 0.56, 0.59 and 0.63 ($\alpha\neq0.50$, asymmetric curves), respectively, as shown in Figs. 4(a−c). While, the first derivative of $f(\alpha)$ or $df(\alpha)/d\alpha$ or $f'(\alpha)$ of the reaction mechanisms is shown in Table 1 with the substitutions of α values by 0.56, 0.59 and 0.63 (from Figs. 4(a−c)). All mentioned parameters were used to substitute into Eq. (30) to determine the corresponding values of A. The calculated A values for the individual peaks 1, 2 and 3 are $(3.91\pm0.049)\times10^6$, $(1.35\pm0.056)\times10^7$ and $(2.15\pm0.044)\times10^7$ s^{-1}, respectively.

According to the basic rate equation, Eq. (12) can be modified to be

$$\frac{d\alpha_i}{dT}=\frac{A_i}{\beta}\exp\left(\frac{-E_i}{RT}\right)f_i(\alpha_i) \tag{38}$$

where the subscript i indicates each individual peak of the single-step reaction of the kinetic parameters. Then, the obtained kinetic parameters were substituted into Eq. (38). Therefore, the thermal solid-state reaction kinetic equations of the synthesized $Mn_{0.90}Co_{0.05}Mg_{0.05}$-$HPO_4\cdot3H_2O$ compound can be expressed as follows:

$$\frac{d\alpha_1}{dT}=\frac{3.91\times10^6}{\beta}\exp\left(\frac{-65.87}{RT}\right)2(1-\alpha_1)^{1/2} \quad (39)$$

$$\frac{d\alpha_2}{dT}=\frac{1.35\times10^7}{\beta}\exp\left(\frac{-78.16}{RT}\right)\frac{1}{[-\ln(1-\alpha_2)]} \quad (40)$$

$$\frac{d\alpha_3}{dT}=\frac{2.15\times10^7}{\beta}\exp\left(\frac{-119.32}{RT}\right)\frac{3(1-\alpha_3)^{2/3}}{2[1-(1-\alpha_3)^{1/3}]} \quad (41)$$

where α_1, α_2 and α_3 are the extents of conversion for the individual peaks 1, 2 and 3, respectively. The experimental and simulated curves between $d\alpha/dT$ and T at a heating rate (β) of 5 °C/min are compared and shown in Figs. S6(a−c) for the first, second and final individual peaks, respectively. The initial conditions for solving Eqs. (39)−(41) were set at α=0.005 [22] and T=80−220 °C (first peak), 80−280 °C (second peak) and 150−550 °C (final peak) to cover the overall reaction of the individual peaks from the thermal solid-state reaction of the studied system in this work. According to Fig. S6, Eqs. (39)−(41) can appropriately describe the nonisothermal solid-state reaction processes of the synthesized hydrate $Mn_{0.90}Co_{0.05}Mg_{0.05}HPO_4{\cdot}3H_2O$.

4.2.4 Thermodynamic function evaluation

According to the Eyring's principle [37] (transition–state or activated complex), the value of the standard entropy change of the activated complex or the standard entropy of transition-state (activated) ΔS^{Θ} relates to the value of the calculated pre-exponential factor A as expressed in Eq. (42):

$$\Delta S^{\Theta}=R\ln\frac{Ah}{e\chi k_B T} \quad (42)$$

where e is the Neper magnitude and equals 2.7183, χ is the transition or transformation factor and equals 1 for the completed reaction, while k_B and h are the Boltzmann (1.3806×10^{-23} J/K) and Planck (6.6261×10^{-34} J·s) constants, respectively. T is the resulted temperature of the peak from the individual DTG curve, which is the same value as that used in the evaluation of A (β= 5 °C/min) in Section 4.2.3.

The standard enthalpy change or the standard heat of transition-state ΔH^{Θ} and the standard Gibbs free energy change of the activated complex or the standard Gibbs free energy of transition-state ΔG^{Θ} can be evaluated according to Eqs. (43) and (44), respectively:

$$\Delta H^{\Theta}=E_\alpha-RT \quad (43)$$

$$\Delta G^{\Theta}=\Delta H^{\Theta}-T\Delta S^{\Theta} \quad (44)$$

The obtained results indicate that the values of ΔS^{Θ} for the first, second and final individual peaks are found to be (−130.27±13.81), (−120.84±12.25) and (−120.23±17.23) J/(K·mol), respectively. The values of the corresponding standard enthalpy of transition-state ΔH^{Θ} are found to be (62.21±3.66), (74.08±4.08) and (113.32±6.00) kJ/mol, whereas those of the standard Gibbs free energy of transition-state ΔG^{Θ} are found to be (57.45±12.42), (59.32±11.28) and (86.95±13.52) kJ/mol, respectively. The negative ΔS^{Θ} values indicate that the transition-state is less disordered compared to the initial state, which can be explained as a "slow" stage [34]. The DTA curves with endothermic peaks agree very well with the positive mark of ΔH^{Θ}. The values of ΔG^{Θ} with positive sign confirm that the thermal solid-state reactions of the studied system are nonspontaneous processes.

5 Conclusions

$Mn_{0.90}Co_{0.05}Mg_{0.05}HPO_4{\cdot}3H_2O$ was thermally decomposed into two sequential steps as dehydration (I, II) and polycondensation processes, respectively, and the final solid-state reaction product was determined as $Mn_{1.8}Co_{0.1}Mg_{0.1}P_2O_7$. The final product showed the thermal stability in the experimental temperature of 750 °C. The excellent crystallinity was recorded at about 710 °C obtained from the complete exothermic DTA peak (at β=5 °C/min). Alternative process for the determination of the conversion value was proposed after using the best fitting deconvolution function. The calculations of the E_α values from the interested kinetic studies of the solid-state reaction were estimated using the iterative integral isoconversional procedure. The first step of the dehydration process showed the overlapped peak in the DTG curve and the Frazer–Suzuki deconvolution function was used to separate the first and second individual peaks. The first, second and final (polycondensation process) individual peaks can be concluded as a single-step kinetic system that is appropriately explained by the unique kinetic parameters. The evaluated reaction mechanism functions of the solid-state reaction obtained by the method of Málek were investigated by comparing the experimental against theoretical plots. The reaction mechanisms for the first, second and final individual peaks are the 2D diffusion (D_2), 3D diffusion (D_3) and contracting cylinder (cylindrical symmetry, R_2) processes, respectively. The related standard thermodynamic functions of the thermal solid-state reaction processes were calculated using the kinetic parameters and were found in great agreement with the experimental results.

Acknowledgements

This work is supported by King Mongkut's Institute of Technology Ladkrabang [KREF146001]. We would like to thank the Advanced Phosphate Materials and Alternative Fuel Energy Research Unit, Department of Chemistry, Faculty of Science, King Mongkut's Institute of Technology Ladkrabang, Thailand. We also thank Assoc. Prof. Dr. Chanaiporn Danvirutai for carefully reading the manuscript.

Supplement

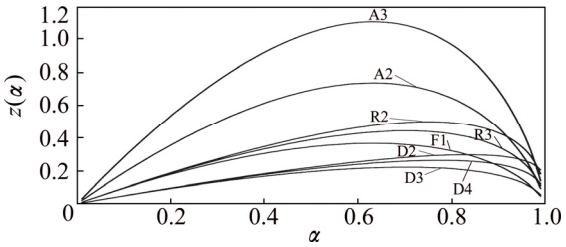

Fig. S1 Certain theoretical $z(\alpha)$ plots for reaction models

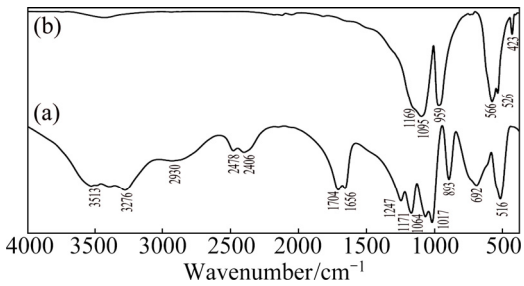

Fig. S2 Recorded FTIR spectra operated at room temperature of synthesized precursor $Mn_{0.90}Co_{0.05}Mg_{0.05}HPO_4{\cdot}3H_2O$ (a) and its thermal solid-state reaction $Mn_{1.8}Co_{0.1}Mg_{0.1}P_2O_7$ (b) in wavenumber range of 4000−370 cm^{-1} by KBr technique

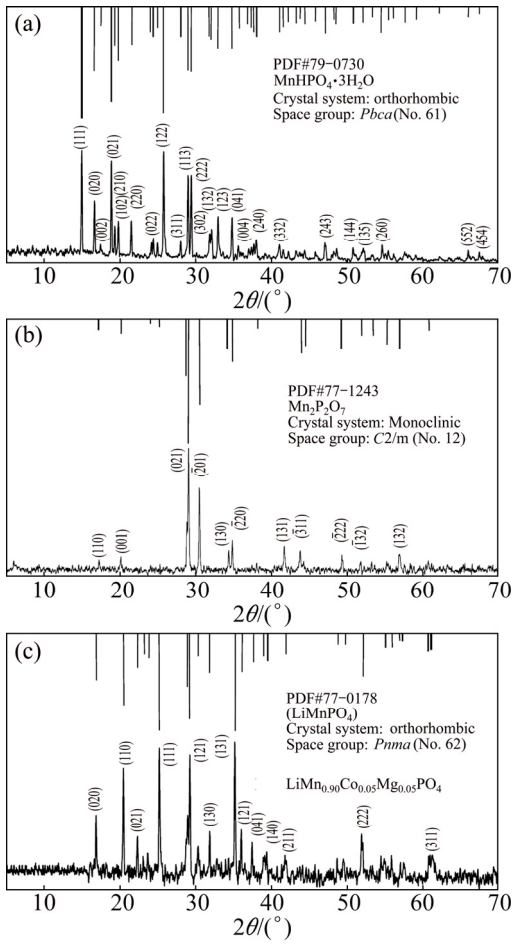

Fig. S3 XRD patterns of $Mn_{0.90}Co_{0.05}Mg_{0.05}HPO_4{\cdot}3H_2O$ compared with that of $MnHPO_4{\cdot}H_2O$ (a), $Mn_{1.8}Co_{0.1}Mg_{0.1}P_2O_7$ compared with that of $Mn_2P_2O_7$ (b), and $LiMn_{0.90}Co_{0.05}$-$Mg_{0.05}PO_4$ compared with that of $LiMnPO_4$ (c)

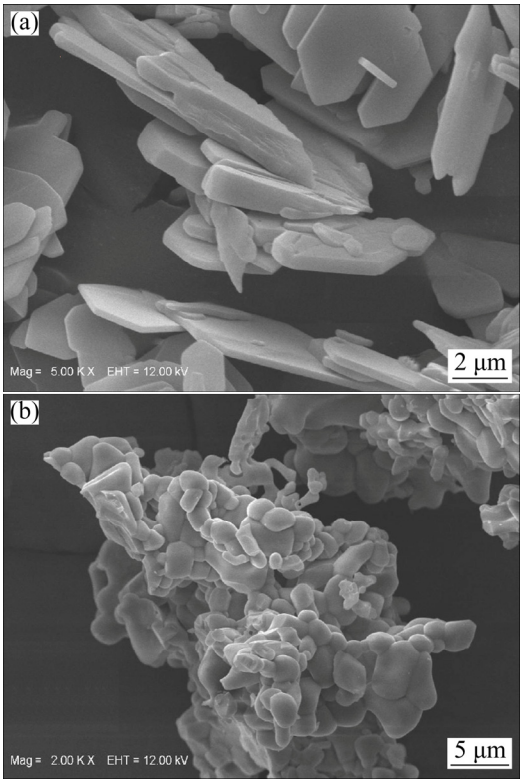

Fig. S4 SEM micrographs of $Mn_{0.90}Co_{0.05}Mg_{0.05}HPO_4{\cdot}3H_2O$ (a) and $Mn_{1.8}Co_{0.1}Mg_{0.1}P_2O_7$ (b) after gold coating technique

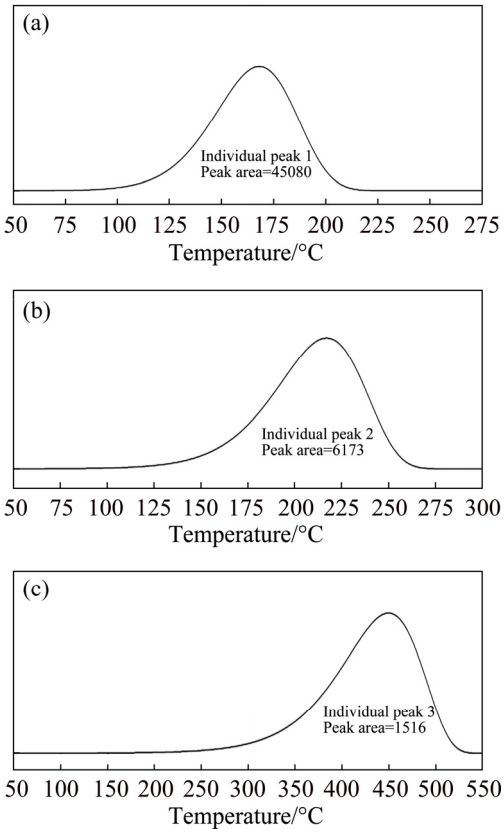

Fig. S5 Three individual DTG peaks including first (a), second (b) and final (c) thermal solid-state reaction processes with their peak areas at heating rate of 5 °C/min obtained from Frazer–Suzuki deconvolution function

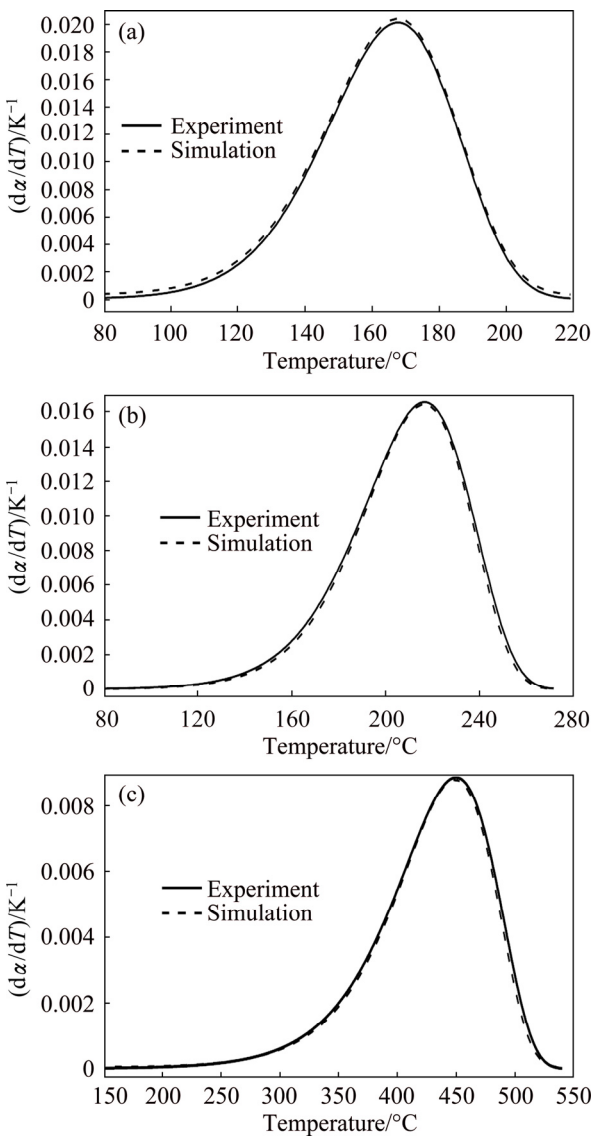

Fig. S6 Experimental and simulation plots of dα/dT versus T of three thermal solid-state reaction processes at heating rate of 5 °C/min: (a) First step, dehydration I; (b) Second step, dehydration II; (c) Final step

References

[1] BOONCHOM B. Kinetic and thermodynamic studies of $MgHPO_4{\cdot}3H_2O$ by non–isothermal decomposition data [J]. Journal of Thermal Analysis and Calorimetry, 2009, 98: 863−871.

[2] SRONSRI C, NOISONG P, DANVIRUTAI C. Solid state reaction mechanisms of the $LiMnPO_4$ formation using special function and thermodynamic studies [J]. Industrial & Engineering Chemistry Research, 2015, 54: 7083−7093.

[3] PANG H, WANG S, SHAO W, ZHAO S, YAN B, LI X, LI S, CHEN J, DU W. Few-layered $CoHPO_4{\cdot}3H_2O$ ultrathin nanosheets for high performance of electrode materials for supercapacitors [J]. Nanoscale, 2013, 5: 5752−5757.

[4] BOONCHOM B, PHUVONGPHA N. Synthesis of new binary cobalt iron pyrophosphate $CoFeP_2O_7$ [J]. Materials Letters, 2009, 63: 1709−1711.

[5] BOONCHOM B, VITTAYAKORN N. Synthesis and ferromagnetic property of new binary copper iron pyrophosphate $CuFeP_2O_7$ [J]. Materials Letters, 2010, 63: 275−257.

[6] SRONSRI C, NOISONG P, DANVIRUTAI C. Synthesis, non-isothermal kinetic and thermodynamic studies of the formation of $LiMnPO_4$ from $NH_4MnPO_4{\cdot}H_2O$ precursor [J]. Solid State Sciences, 2014, 32: 67−75.

[7] SRONSRI C, NOISONG P, DANVIRUTAI C. Synthesis, characterization and vibrational spectroscopic study of Co, Mg co–doped $LiMnPO_4$ [J]. Spectrochimica Acta Part A: Molecular and Biomolecular Spectroscopy, 2016, 153: 436−444.

[8] PEREJÓN A, SÁNCHEZ–JIMÉNEZ P E, CRIADO J M, PÉREZ–MAQUEDA L A. Kinetic analysis of complex solid-state reactions: A new deconvolution procedure [J]. Journal of Physical Chemistry B, 2011, 115: 1780−1791.

[9] FRIEDMAN H L. Kinetics of thermal degradation of char-forming plastics from thermogravimetry: Application to a phenolic plastic [J]. Journal of Polymer Science: Polymer Symposia, 1964, 6: 183−195.

[10] KHAWAM A, FLANAGAN D R. Complementary use of model-free and modelistic methods in the analysis of solid–state kinetics [J]. Journal of Physical Chemistry B, 2005, 109: 10073−10080.

[11] GOTOR F J, CRIADO J M, MÁLEK J, KOGA N. Kinetic analysis of solid–state reactions: The universality of master plots for analyzing isothermal and nonisothermal experiments [J]. Journal of Physical Chemistry A, 2000, 104: 10777−10782.

[12] SEMPERE J, NOMEN R, SERRA R, SORAVILLA J. The NPK method: An innovative approach for kinetic analysis of data from thermal analysis and calorimetry [J]. Thermochimica Acta, 2002, 388: 407−414.

[13] SÁNCHEZ–JIMÉNEZ P E, PÉREZ–MAQUEDA L A, PEREJÓN A, CRIADO J M. Combined kinetic analysis of thermal degradation of polymeric materials under any thermal pathway [J]. Polymer Degradation and Stability, 2009, 94: 2079−2085.

[14] VYAZOVKIN S, BURNHAM A K, CRIADO J M, PÉREZ–MAQUEDA L A, POPESCU C, SBIRRAZZUOLI N. ICTAC kinetics committee recommendations for performing kinetic computations on thermal analysis data [J]. Thermochimica Acta, 2011, 520: 1−19.

[15] SRONSRI C, BOONCHOM B. Deconvolution technique for the kinetic analysis of a complex reaction and the related thermodynamic functions of the formation of $LiMn_{0.90}Co_{0.05}Mg_{0.05}PO_4$ [J]. Chemical Physics Letters, 2017, 690: 116−128.

[16] SRONSRI C, BOONCHOM B. Synthesis, characterization, vibrational spectroscopy, and factor group analysis of partially metal-doped phosphate materials [J]. Spectrochimica Acta Part A: Molecular and Biomolecular Spectroscopy, 2018, 194: 230−240.

[17] CULLITY B D. Elements of X–ray diffraction [M]. 2nd ed. MA: Addison–Wesley Publishing, 1978.

[18] BARBADILLO F, FUENTES A, NAYA S, CAO R, MIER J L, ARTIAGA R. Evaluating the logistic mixture model on real and simulated TG curves [J]. Journal of Thermal Analysis and Calorimetry, 2007, 87: 223−227.

[19] CAI J M, ALIMUJIANG S. Kinetic analysis of wheat straw oxidative pyrolysis using thermogravimetric analysis: Statistical description and isoconversional kinetic analysis [J]. Industrial & Engineering Chemistry Research, 2009, 48: 619−624.

[20] JANKOVIC B, ADNADEVIC B, KOLAR–ANIC L, SMICIKLAS I. The non–isothermal thermogravimetric tests of animal bones combustion. Part II. Statistical analysis: Application of the Weibull mixture model [J]. Thermochimica Acta, 2010, 505: 98−105.

[21] WEIBULL W. A statistical distribution function of wide applicability [J]. Journal of Applied Mechanics, 1951, 18: 293−297.

[22] LIU S H, SHU C M. Advanced technology of thermal decomposition for AMBN and ABVN by DSC and VSP2 [J]. Journal of Thermal Analysis and Calorimetry, 2015, 121: 533−540.

[23] SATO Y. Evaluation of the hazard of heat generation by oxidation of materials using a differential-type adiabatic calorimeter [J]. Journal of Thermal Analysis and Calorimetry, 2016, 123: 1851−1859.

[24] GALWAY A K. Solid state reaction kinetics, mechanisms and catalysis: A retrospective rational review [J]. Reaction Kinetics, Mechanisms and Catalysis, 2015, 114: 1−29.

[25] L'VOV B V. Thermal decomposition of solids and melts [M]. Berlin: Springer, 2007.

[26] L'VOV B V. Activation effect in heterogeneous decomposition reactions: fact or fiction? [J]. Reaction Kinetics, Mechanisms and Catalysis, 2014, 111: 415−429.

[27] L'VOV B V. On the way from the activation model of solid decomposition to the thermochemical model [J]. Reaction Kinetics, Mechanisms and Catalysis, 2015, 116: 1−18.

[28] BUDRUGEAC P, SEGAL E. Some methodological problems concerning nonisothermal kinetic analysis of heterogeneous solid–gas reactions [J]. International Journal of Chemical Kinetics, 2001, 33: 564−573.

[29] BUDRUGEAC P. Some methodological problems concerning the kinetic analysis of non–isothermal data for thermal and thermo-oxidative degradation of polymers and polymeric materials [J]. Polymer Degradation and Stability, 2005, 89: 265−273.

[30] VYAZOVKIN S. Modification of the integral isoconversional method to account for variation in the activation energy [J]. Journal of Computational Chemistry, 2001, 22: 178−183.

[31] VYAZOVKIN S, DOLLIMORE D. Linear and nonlinear procedures in isoconversional computations of the activation energy of nonisothermal reactions in solids [J]. Journal of Chemical Information and Modeling, 1996, 36: 42−45.

[32] BUDRUGEAC P. Differential non-linear isoconversional procedure for evaluating the activation energy of non-isothermal reactions [J]. Journal of Thermal Analysis and Calorimetry, 2002, 68: 131−139.

[33] CAI J, CHEN S. A new iterative linear integral isoconversional method for the determination of the activation energy varying with the conversion degree [J]. Journal of Computational Chemistry, 2009, 30: 1986−1991.

[34] SRONSRI C, NOISONG P, DANVIRUTAI C. Thermal decomposition kinetics of $Mn_{0.9}Co_{0.1}HPO_4{\cdot}3H_2O$ using experimental–model comparative and thermodynamic studies [J]. Journal of Thermal Analysis and Calorimetry, 2017, 127: 1983−1994.

[35] MÁLEK J. A computer program for kinetic analysis of non–isothermal thermoanalytical data [J]. Thermochimica Acta, 1989, 138: 337−346.

[36] SRONSRI C, NOISONG P, DANVIRUTAI C. Isoconversional kinetic, mechanism and thermodynamic studies of the thermal decomposition of $NH_4Co_{0.8}Zn_{0.1}Mn_{0.1}PO_4{\cdot}H_2O$ [J]. Journal of Thermal Analysis and Calorimetry, 2015, 120: 1689−1701.

[37] ROONEY J J. Eyring transition-state theory and kinetics in catalysis [J]. Journal of Molecular Catalysis A: Chemical, 1995, 96: L1−L3.

基于反卷积过程新算法分析 $Mn_{0.90}Co_{0.05}Mg_{0.05}HPO_4{\cdot}3H_2O$ 固相反应复杂过程的热动力学及相关热力学函数

Chuchai SRONSRI, Banjong BOONCHOM

Advanced Phosphate Materials and Alternative Fuel Energy Research Unit, Department of Chemistry, Faculty of Science, King Mongkut's Institute of Technology Ladkrabang, Bangkok, Thailand

摘　要：合成 $Mn_{0.90}Co_{0.05}Mg_{0.05}HPO_4{\cdot}3H_2O$ 的热固相反应过程存在 3 个独立的峰，分别对应于脱水Ⅰ、脱水Ⅱ和缩聚 3 个过程。提出一种根据单个 DTG 峰的峰面积计算转化率的新方法，即采用 Frazer−Suzuki 反卷积函数进行最优拟合。采用迭代积分等转化率方程计算 3 个峰的表观活化能 E_α 分别为 65.87、78.16 和 119.32 kJ。保证每个独立的峰都是一个具有特征动力学参数的单步骤动力学体系，通过实验曲线与模拟曲线的比较，确定反应机理函数。结果表明，第一、第二和最后的独立峰分别为球对称的二维扩散机理(D_2)、球对称的三维扩散机理(D_3)和收缩圆柱机理(圆柱对称，R_2)。根据 E_α 值和反应机理，计算出指数前因子分别为 3.91×10^6, 1.35×10^7 和 2.15×10^7 s。确定过渡态(活化)配合物的标准热力学函数，结果与实验数据吻合良好。

关键词：固相反应；算法；复杂反应；Frazer−Suzuki 函数；实验和模拟曲线

(Edited by Bing YANG)